

## Design and characterization of three light-weight multi-principal-element alloys potentially candidates as high-entropy alloys

Pablo Pérez<sup>a</sup>, Gerardo Garcés<sup>a</sup>, Enrique Frutos-Myro<sup>a</sup>, Juan M. Antoranz<sup>b</sup>,  
Sophia Tsipas<sup>c</sup>, Paloma Adeva<sup>a,✉</sup>

<sup>a</sup>Centro Nacional de Investigaciones Metalúrgicas (CENIM, CSIC), Avda. Gregorio del Amo 8, 28040 Madrid, Spain

<sup>b</sup>Universidad Politécnica de Madrid (UPM – ETSIAE), Plaza de Cardenal Cisneros 3, 28040 Madrid, Spain

<sup>c</sup>Universidad Carlos III de Madrid, IAAB, Avda. de la Universidad 30, 28911 Leganés, (Madrid) Spain

(✉Corresponding author: [adeva@cenim.csic.es](mailto:adeva@cenim.csic.es))

Submitted: 23 January 2019; Accepted: 23 May 2019; Available On-line: 29 July 2019

**ABSTRACT:** The feasibility of preparing high entropy alloys in the Al-Sc-Ti-V-Cr system has been evaluated taking into account the different criteria reported in the literature. Based on such criteria, three Al-Sc-Ti-V-Cr alloys were chosen with contents of each element varying from 10 to 35 at. %, and prepared by arc melting. All alloys exhibit a two-phase dendritic microstructure, with the major dendritic phase being a bcc solid solution enriched in Ti, V, or Cr. Scandium is strongly rejected from the dendrites towards the interdendritic regions to form Al<sub>2</sub>Sc in the three alloys. The bcc solid solution dendrites become harder with high Ti content and lower with high Cr content. The toughness of the alloys depends on the hardness of the dendrites, with alloys with harder dendrites becoming more brittle. The results indicate that neither empirical criteria used nor THERMOCALC calculus tool can predict properly the formation of a single solid solution nor the nature of the existing phases respectively.

**KEYWORDS:** High entropy alloys; Microanalysis; Microscopy; Microstructure; Toughness

**Citation/Citar como:** Pérez, P.; Garcés, G.; Fruto-Myro, E.; Antoranz, J.M.; Tsipas, S.; Adeva, P. (2019). “Design and characterization of three light-weight multi-principal-element alloys potentially candidates as high-entropy alloys”. *Rev. Metal.* 55(3): e147. <https://doi.org/10.3989/revmetalm.147>

**RESUMEN:** *Diseño y caracterización de tres aleaciones multiprincipales ligeras potencialmente candidatas a aleaciones de alta entropía.* En este trabajo se estudia la posibilidad de preparar aleaciones de alta entropía del sistema Al-Sc-Ti-V-Cr. Para ello se han seleccionado los elementos y la composición utilizando los criterios conocidos y disponibles en la literatura y se han preparado mediante fusión por arco tres aleaciones con contenidos que varían entre el 10 y 35 at.%. Las tres aleaciones tienen una microestructura dendrítica bifásica similar, siendo las dendritas una solución sólida bcc enriquecida en Ti, V o Cr. El escandio aparece únicamente en el espacio interdendrítico formando el intermetálico Al<sub>2</sub>Sc. La dureza de las dendritas crece con el contenido en Ti y se hace menor a medida que es mayor el contenido en Cr. Además, la tenacidad de las aleaciones depende de la dureza de las dendritas siendo ésta mayor cuanto más blandas son las dendritas. Los resultados obtenidos demuestran que ni los criterios empíricos utilizados ni los cálculos mediante THERMOCALC permiten predecir la formación de una única solución sólida ni la naturaleza de las fases observadas experimentalmente.

**PALABRAS CLAVE:** Alta entropía; Microanálisis; Microestructura; Microscopía; Tenacidad

**ORCID ID:** Pablo Pérez Zubiaur (<https://orcid.org/0000-0002-4218-2573>); Gerardo Garcés (<https://orcid.org/0000-0002-6896-7475>); Enrique Frutos-Myro (<https://orcid.org/0000-0002-3146-2350>); Juan M. Antoranz (<https://orcid.org/0000-0002-7982-0188>); Sophia Tsipas (<https://orcid.org/0000-0001-7590-2795>); Paloma Adeva (<https://orcid.org/0000-0002-9111-8893>)

**Copyright:** © 2019 CSIC. This is an open-access article distributed under the terms of the Creative Commons Attribution 4.0 International (CC BY 4.0) License.

## 1. INTRODUCTION

The high-entropy alloys (HEA) are receiving great scientific attention over the last decade in view of the good balance of properties (Cantor *et al.*, 2004; Cantor, 2011; Zhang *et al.*, 2014). Recent revisions on this class of metallic materials show evidences the discrepancies and existing controversy about the definition of HEAs (Pickering and Jones, 2016; Miracle and Senkov, 2017). One of the most accepted definition is that HEAs alloys are not based around a single major element but rather contain several ( $\geq 5$ ) major elements, present each in concentrations between about 5 and 35 at.%, that are expected to stabilize a solid solution with simple crystal structure in view of the high mixing entropy. Such lattices suffer significant lattice distortion due to differences in size among the atoms present, and are hence expected to show good strength and wear resistance, with low diffusivity and good thermal stability (Wu *et al.*, 2006; Cantor, 2011; Zhang *et al.*, 2014). Apart from the requirement of high configurational entropy of mixing ( $\Delta S_{\text{mix}}$ ) and low mixing enthalpy ( $\Delta H_{\text{mix}}$ ) considerable attention has been devoted to understanding what other parameters determine the stability of solid solutions in HEAs (Yeh *et al.*, 2004; Zhang *et al.*, 2008; Ren *et al.*, 2010; Guo and Liu, 2011; Yang and Zhang, 2012; Zhang and Fu, 2012; Poletti and Battezzati, 2014; Zhang, *et al.*, 2014; Lu *et al.*, 2015). It has been widely used the three Hume-Rothery rules which are based on three parameters: average size difference ( $\delta$ ) between the atoms present, electronegativity difference ( $\Delta\chi$ ) and the valence electron concentration (VEC). Such criteria are not completely satisfactory to predict solid solution formation, however, and research continues to develop other possible criteria. Ye *et al.* (2015) proposed a new elastic strain energy parameter coupled with the mixing enthalpy. Toda-Caraballo and Rivera-Díaz-del-Castillo (2016) propose two new parameters, the interatomic spacing mismatch ( $\text{sm}$ ) and bulk modulus mismatch ( $\text{Km}$ ).

Despite a large amount of reported work on HEAs, very few HEAs are completely single phase solid solutions. Often minor amounts of second phases or two-phase dendrite-plus-eutectic structure are found (Cantor *et al.*, 2004; Zhang and Fu, 2012; Yue *et al.*, 2013; Zhang *et al.*, 2014; Cantor *et al.*, 2005). The thermal stability of the simple solid solution is also unclear, with subsequent annealing leading to phase decomposition or total dissolution (Zhang and Fu, 2012). To date, research in HEAs has been carried out mainly on alloys containing high concentrations of transition metals with high densities, typically above 7–8  $\text{g}\cdot\text{cm}^{-3}$ . Numerous studies have been reported regarding in these series of alloys, as found in the review by Pickering and Jones (2016), but research focused in light high entropy alloys is still scarce. Some of them are that

by Youssef *et al.* (2015) in AlLiMgScTi but most of them are included in the review by Kumar and Gupta (2016).

The present study set out to obtain low density HEAs using conventional melting and casting techniques to avoid complex processing methods and/or contamination (as it is often the case for mechanical alloying or rapid solidification techniques). The objective was to achieve single phase alloys with simple crystal structures with densities close to  $5\text{ g}\cdot\text{cm}^{-3}$ . As a guide for likely suitable chemical compositions, standard thermodynamic data (Takeuchi and Inoue, 2005) and the criteria from Guo and Liu (2011) describing heat of mixing, atomic misfit, or electronic densities were considered. These criteria may be summarized as follows:

- (i) a high entropy of mixing ( $\Delta S_{\text{mix}}$ ), of the order of 11–19 J/K/mol;
- (ii) a low value of atomic misfit parameter ( $\delta$ ), in the range 0 to 8%;
- (iii) a low value of heat of mixing ( $\Delta H_{\text{mix}}$ ), of the order of -22 to 7  $\text{kJ}\cdot\text{mol}^{-1}$ ;
- (iv) a moderate electronegativity difference ( $\Delta\chi$ ), in the range 0.1 to 0.35;
- (v) a high value of valency electron concentration (VEC), about 5–9.

After evaluation of a wide range of elemental compositions, according to the mentioned criteria, three alloys belonging to the AlScTiVCr system were chosen as possible candidates as light-weight HEAs.

Figure 1 shows the results of such thermodynamic calculations for heat of mixing ( $\Delta H_{\text{mix}}$ ) versus atomic misfit parameter for many alloys in the AlScTiVCr family, as well as the three alloys selected for the experimental study. Alloys 1 and 3 were chosen because of their lowest values of the misfit parameter  $\delta$  while the smallest value of  $\Delta H_{\text{mix}}$  was the criterion followed for selecting the alloy 2. Also indicated in this figure are those compositions where the density changes from below  $5\text{ g}\cdot\text{cm}^{-3}$  to above that value.

In this work, after characterizing the microstructure and mechanical properties of the three AlScTiVCr alloys, calculus of new parameters proposed more recently are compared with the conventional used in this work. Furthermore, predictions of phases present at high temperature were done by means of *Thermocal* software and the results compared and discussed with experimental observations.

## 2. EXPERIMENTAL PROCEDURE

Three Al-Sc-Ti-V-Cr alloys, whose nominal compositions are listed in Table 1, were prepared from pure elements in an arc furnace under argon atmosphere. Each sample, weighing about 5 g, was

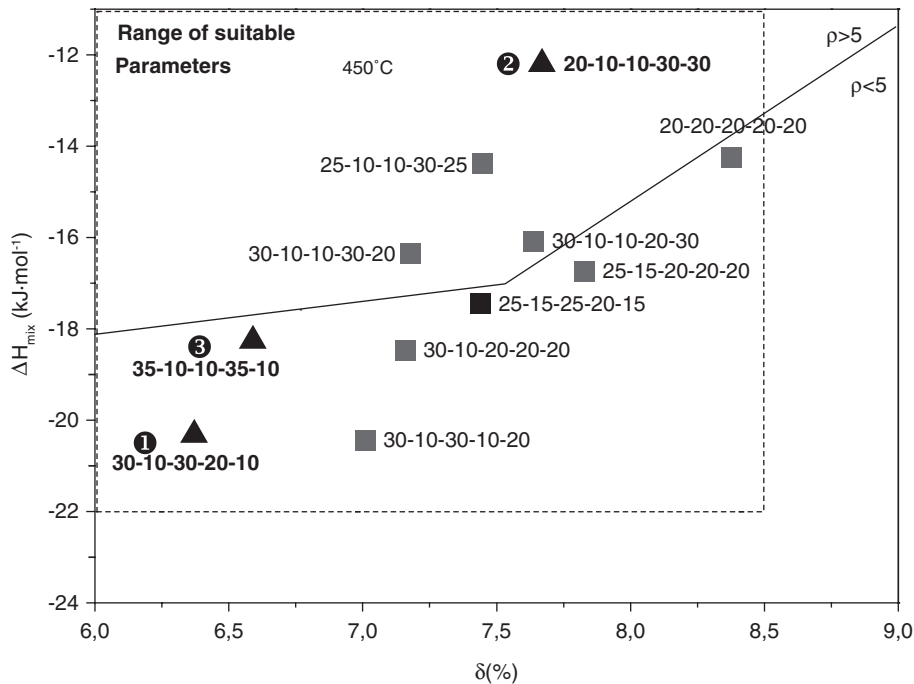


FIGURE 1. Map of  $\Delta H_{\text{mix}}$  and  $\delta$  showing the influence of composition variations on parameters in the Al-Sc-Ti-V-Cr system. Compositions are indicated as atomic percent in the order indicated. ■ Indicate the compositions of a wide range of alloys, and ▲ the alloys selected for experimental study. The range of suitable thermodynamic parameters for finding HEAs is found within the region enclosed by dotted lines. The composition range where a density of  $5 \text{ g}\cdot\text{cm}^{-3}$  is expected, is indicated by the solid line.

TABLE 1. Nominal composition of the three alloys, at. and wt. %

	Al	Sc	Ti	V	Cr
<b>Alloy 1</b> at. %	30	10	30	20	10
wt. %	19.1	10.6	33.9	24.1	12.3
<b>Alloy 2</b> at. %	20	10	10	30	30
wt. %	11.8	9.9	10.5	33.5	34.2
<b>Alloy 3</b> at. %	35	10	10	35	10
wt. %	22.6	10.8	11.5	42.7	12.5

re-melted five times turning over the button each time, to ensure homogeneous composition which was confirmed by Energy Dispersive X-ray (EDX) microanalysis at several areas.

Phase and microstructural characterization was carried out by X-ray diffraction, Scanning Electron Microscopy (SEM) and EDS microanalysis, and by electron backscattering diffraction (EBSD) carried out in a SEM. Observations of samples by backscattered electron images were conducted at 10 and 15 kV but EDS microanalysis was always carried out at 15 kV. All the microanalytical results presented are the average at least of five separated areas. X-ray diffraction analysis was carried out with a Bruker AXS D8 Diffractometer using Co radiation at 40 kV and 30 mA on a polished section.

Thermal characterization of the alloys, especially to determine the temperature where melting started, was done by differential thermal analysis (DTA) in argon atmosphere using a heating rate of  $10 \text{ K}\cdot\text{min}^{-1}$ .

Quasi-binary diagrams were simulated using *Thermocalc* software with SSOL5 database (Andersson *et al.*, 2002)

The macrohardness of the alloys, as well as the microhardness of different phases and an estimate of fracture toughness, were determined from Vickers hardness imprints on polished samples. Loads of 2 kg and 100 g, respectively, were used for macro and micro hardness testing, taking an average of 5 indentations. Fracture toughness,  $K_{\text{Q}}$ , was estimated from the length of cracks generated at the corners of indentations at progressively higher loads, ranging from 200 g to 2 kg, noting the load when cracking began, and using standard relationships (Anstis *et al.*, 1981; Morris *et al.*, 1998) to determine toughness from the crack length at an applied load of 2 kg.

### 3. RESULTS

#### 3.1. Microstructural characterization

The three alloys have a homogeneous dendritic structure as seen in the backscattered electron images of Fig. 2. The dendrites always appear in

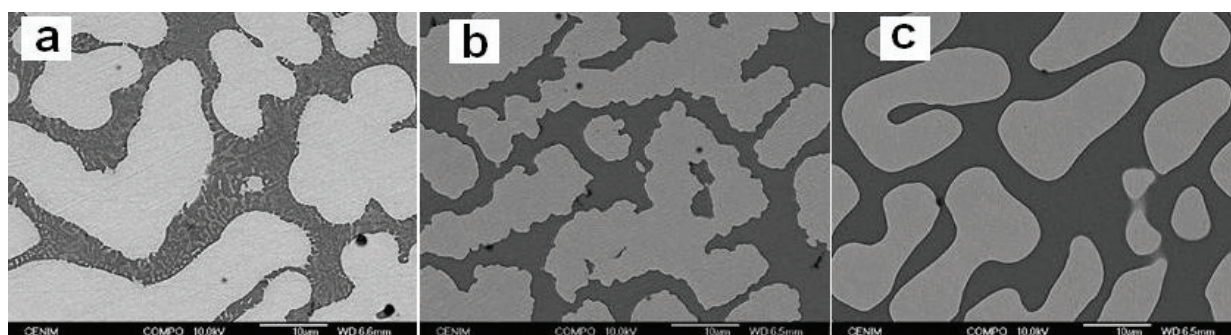


FIGURE 2. SEM images taken in Back-scattered electron images (BSE) showing dendritic microstructure for the three alloys: a, b, c correspond to alloys 1, 2 and 3, respectively.

TABLE 2. Semiquantitative microanalysis results of chemical compositions of phases in the three alloys, as determined by EDS (at. %).  $V_v$  indicates the volume fraction

Alloy	Phase/Elements (at. %)	Al	Sc	Ti	V	Cr
1	Dendrite, $V_v=79\%$	24.5	3.4	37.6	24	10.5
	Inter-dendritic dark	36.5	28.8	14.2	10.4	10.1
	Inter-dendritic light	34.6	23.2	27	9.6	5.6
2	Dendrite, $V_v=68\%$	12.7	1	8.7	41.6	36
	Inter-dendritic	33.3	29.8	9.4	8.9	18.6
3	Dendrite, $V_v=65\%$	25.3	1.5	13.6	47.6	12
	Inter-dendritic	43.4	30.7	5.9	12.3	7.7

light contrast, indicating a high content of the heavier metals, while the darker, interdendritic phase shows some weak internal contrast for alloy 1, indicative of the existence of two phases, possibly as a binary eutectic mixture. Such phase separation was not found for alloys 2 and 3. The volume fraction of the dendrites was determined by quantitative metallography, counting on a point grid on several low-magnification images. Dendrite volumes of 79%, 68% and 65%, respectively, were deduced for alloys 1, 2 and 3, as indicated in Table 2, while the dendrite arm spacing appeared about constant, near 10 microns, for all three alloys.

The chemical composition of both dendrites and the interdendritic phase was determined by qualitative and semiquantitative analysis. According to X-ray map of alloy 1, shown in Fig. 3, the dendrites are enriched in Ti and V while a Ti-rich phase (bright phase) and a dark interdendritic phase enriched in Al and Sc are present at the interdendritic arms. The analyses reported in Table 2, however, indicate that dendrites are a solid solution of V, Al and Cr in Ti. Sc is strongly rejected from the dendrites into the interdendritic region. The high amounts of Sc and Al observed in the bright Ti-rich phase is related to the matrix effect due to its very fine size.

For alloy 2, the dendrites are a solid solution of Al and Ti in V and Cr, while again the Sc is strongly

rejected from the dendrites to the interdendritic phase observing an Al-Sc single phase. Finally, the X-ray maps for alloy 3 (Fig. 4) shows dendrites enriched in V with Cr and minor amounts of Al and Ti while the interdendritic phase is once again enriched in Al and Sc, containing small amounts of V, Cr and Ti with no signs of any decomposition. The chemical analysis (Table 2) is consistent with the X-ray maps but dendrites seem to be a V-Al rich matrix containing in solid solution Cr and Ti.

X-ray diffraction patterns of Fig. 5 evidence that the major phase, corresponding to the dendrites, is a bcc phase. The lattice parameter of this bcc phase changes somewhat with alloy chemistry since the identified phases were Ti-V, V and Al-V for dendrites of alloys 1, 2 and 3, respectively. Moreover, it is noticed a slight displacement of the theoretical positions of the diffraction peaks of these phases due to the modification of the lattice parameter by the elements present in solid solution, as inferred from semiquantitative analysis in Table 2. Examination of these changes confirms that, for example, an increase in the Cr content tends to shrink the lattice parameter. Additional diffraction peaks were visible for each alloy, see Fig. 5, which must correspond to the interdendritic phases, but whose identification could not be unequivocally done. From these diffraction peaks, the additional phases present for

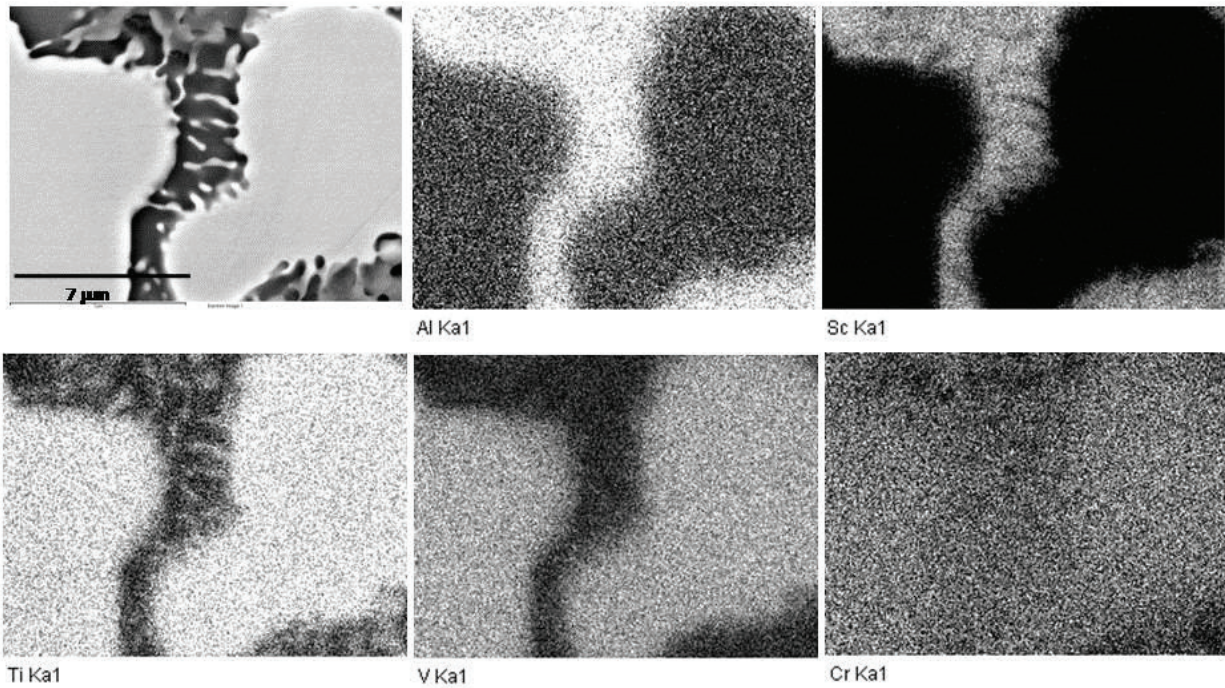


FIGURE 3. X-ray maps of Al, Sc, Ti, V and Cr (using Ka lines) for dendrites and interdendritic phase in alloy 1.

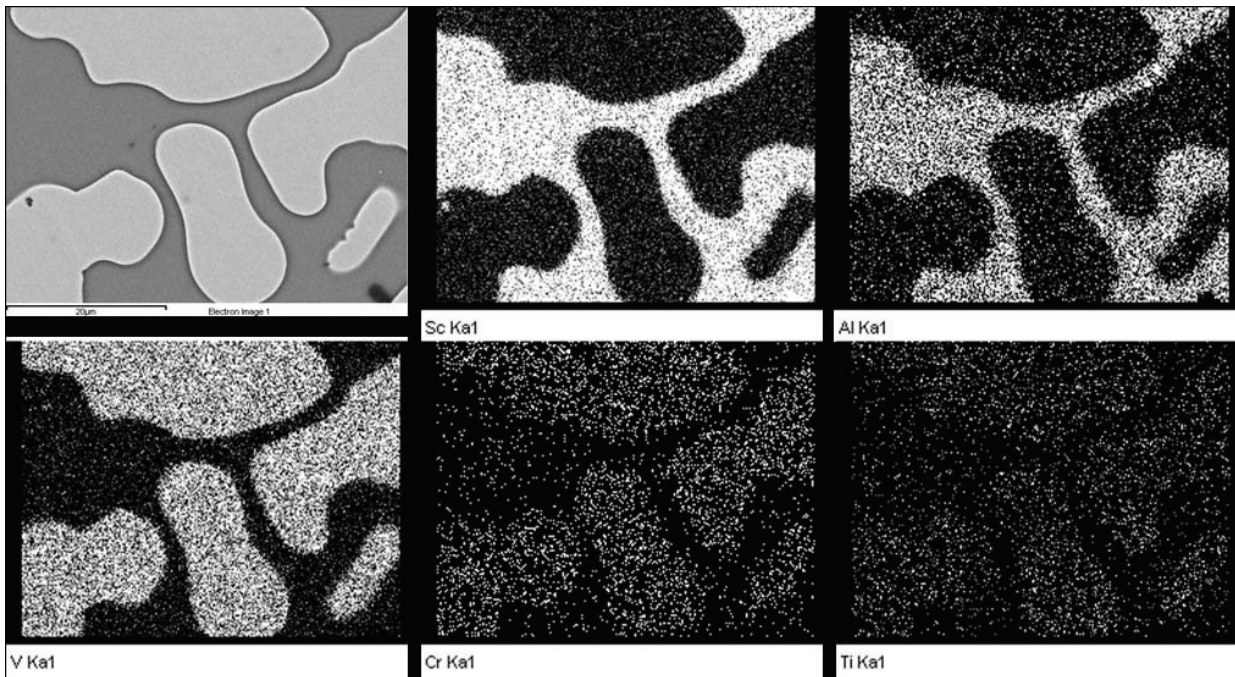


FIGURE 4. X-ray maps of Sc, Al, V, Cr and Ti (using Ka lines) for dendrites and interdendritic phase in alloy 3.

alloy 1 are identified as  $Al_2Sc$  and/or  $AlSc$  (dissolving other elements) and  $\alpha$ -Ti. This two-phase structure could be formed as a binary eutectic reaction by the transformation of a liquid very enriched in Al, Sc and Ti, with small quantities of Cr and V, into

Ti+ $AlSc$  or  $Al_2Sc$ . For alloys 2 and 3, both  $Al_2Sc$  and  $AlSc$  are also identified.

To confirm X-ray identification of phases on the basis of X-ray diffraction data, EBSD maps were obtained. At least three maps were obtained for

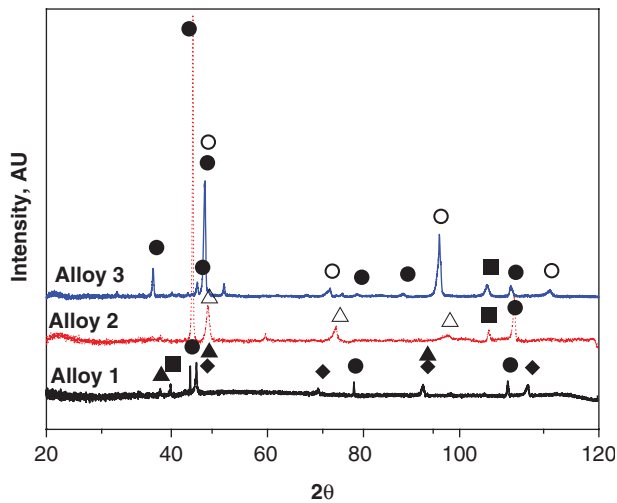


FIGURE 5. X-ray Diffraction patterns of the three alloys.  $\blacklozenge$  Ti-V (bcc,  $a = 3.14 \text{ \AA}$ );  $\triangle$  V (bcc,  $a = 3.03 \text{ \AA}$ );  $\circ$  Al-V (bcc,  $a = 3.074 \text{ \AA}$ );  $\blacktriangle$   $\alpha$ -Ti (hcp,  $a = 2.92 \text{ \AA}$  and  $c = 4.67 \text{ \AA}$ );  $\blacksquare$  AlSc (bcc,  $a = 3.45 \text{ \AA}$ );  $\bullet$   $\text{Al}_2\text{Sc}$  (fcc,  $a = 7.56 \text{ \AA}$ )

each sample to confirm the homogeneous character of alloys since the maps were similar everywhere. As can be seen in Fig. 6, the bcc phase and  $\text{Al}_2\text{Sc}$  were indexed leading to an almost complete description of the materials. It is also clear in Fig. 6 that for alloy 1 the interdendritic region is composed of a eutectic-like mixture of bcc-Ti and  $\text{Al}_2\text{Sc}$ .

To determine the incipient melting temperature of the three alloys, DTA tests from room temperature up to  $1400 \text{ }^\circ\text{C}$  at a heating rate of  $10 \text{ Kmin}^{-1}$  were done. An endothermic reaction occurs at  $1264 \text{ }^\circ\text{C}$ ,  $1324 \text{ }^\circ\text{C}$  and  $1328 \text{ }^\circ\text{C}$  for alloys 1, 2 and 3, respectively (Fig. 7), which have to be related to the melting of the interdendritic phase.

### 3.2. Mechanical characterization: Hardness and Toughness

Microhardness testing was carried out in an attempt to determine the hardness of the dendrite and the interdendritic material, while hardness

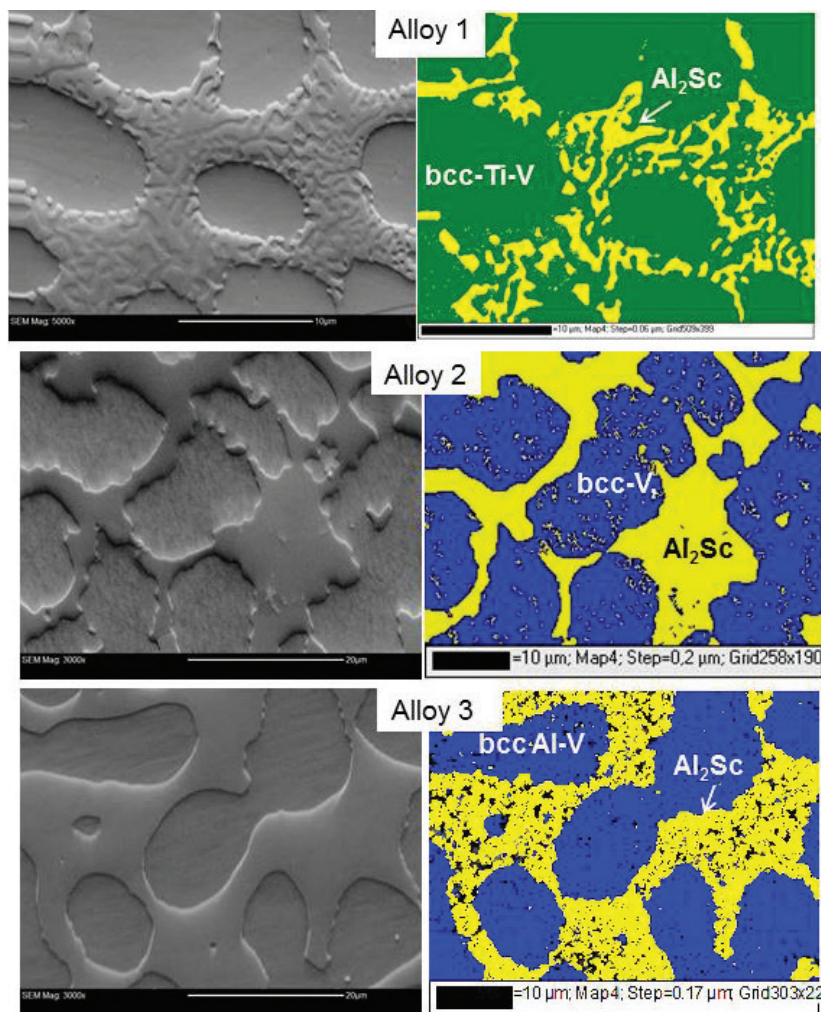


FIGURE 6. Phases identified by EBSD. Occasional small white and grey areas correspond to points not indexed because their Kikuchi maps were diffuse.

testing at progressively higher loads was carried out to obtain information on the toughness of the alloys.

Test results, shown in Table 3, confirmed the higher hardness of the interdendritic material (with the exception of alloy 1, where the larger volume fraction of dendrites meant that the interdendritic region was too fine to allow the determination of a hardness value). The solid solution constituting dendrites of alloy 1 was the hardest while that of alloy 2 was softest according to microhardness testing. Hardness testing shown that alloy 1 is the hardest, in agreement with the highest values of microhardness of dendrites in this alloy, and alloy 3 the softest.

Hardness testing at progressively higher loads showed the onset of fine cracking, initially within the interdendritic material, at relatively low load for alloys 1 and 3, and only at higher loads for alloy 2 (see Table 3). Figure 8 shows examples of the onset and propagation of cracks, most easily in the interdendritic phase and from the corners of the indent. The measurement of crack lengths at high loads, where the crack dimensions are similar to those of the imprint, allows the estimation of fracture toughness, as indicated also in Table 3. Alloy 1, where

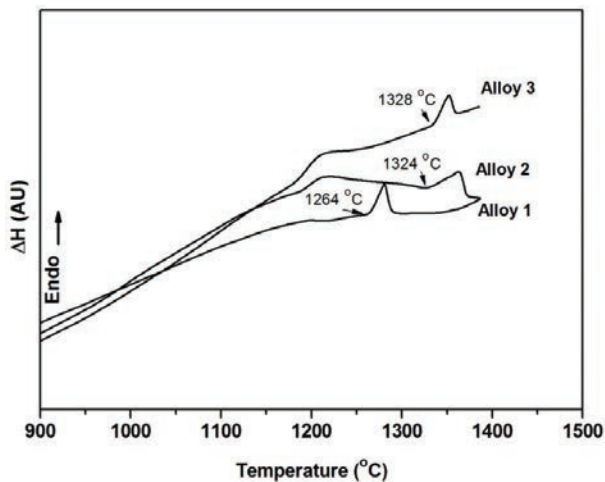


FIGURE 7. DTA curves for the three alloys obtained during heating at a rate of  $10 \text{ K} \cdot \text{min}^{-1}$ .

cracking began early in the interdendritic material, had a low toughness, while alloy 2, requiring much higher loads for crack initiation, had a good toughness value.

#### 4. DISCUSSION

The present study has shown that it is possible to obtain alloys where the predominant phase is a simple bcc solid solution, constituting around 65–80% of the material, corresponding the rest to intermetallic Al-Sc compounds. Low densities, close to  $5 \text{ g} \cdot \text{cm}^{-3}$ , are found for such alloys.

It is of interest to compare the validity of the various prediction criteria with experimental result for the present alloys. Firstly, low values of the VEC parameter, below 5, have been found for all alloys which is consistent in predicting that the solid solution phase will have the bcc structure, not the fcc structure, but that this parameter alone is no enough in determining whether a HEA will be obtained. Most often the ability to form an essentially single phase solid solution is related to moderate values of the parameters  $\Delta H_{\text{mix}}$  (below about  $-20 \text{ kJ} \cdot \text{mol}^{-1}$ ) and  $\delta$  (below 4–8%) (Yeh *et al.*, 2004; Zhang *et al.*, 2008; Ren *et al.*, 2010; Guo and Liu, 2011; Yang and Zhang, 2012; Zhang and Fu, 2012; Zhang, *et al.*, 2014; Lu *et al.*, 2015). The three alloys studied here have suitable values of these two criteria (see Table 4). Recently other parameters such as  $\Omega$  and  $\gamma$  seem to be more precise to predict phase regions in HEAs (Yang and Zhang, 2012; Yang *et al.*, 2012; Zhang *et al.*, 2012; Fu *et al.*, 2016). Thus,  $\Omega$  parameter considers the entropy of mixing, the average melting temperature and the enthalpy of mixing. This parameter combined with  $\delta$  parameter, being values of  $\Omega$  higher than 1.1 and  $\delta$  lower than 6.6%, the formation of a high-entropy stabilized solid solution phase can be predicted if values of both parameters are accomplished simultaneously. As seen in Table 3, alloys 1 and 2 don't fulfill this rule while alloy 3 has a value of both parameters in the limit of criteria although our experimental results indicate also a two-phase alloy. On the other hand,  $\gamma$  parameter, which considers the packing angles

TABLE 3. Results of hardness and toughness testing

	Alloy 1	Alloy 2	Alloy 3
Microhardness (100 g) Dendrites	679 Hv	519 Hv	554 Hv
Microhardness (100 g) Interdendritic phase	(too fine)	664 Hv	696 Hv
Hardness (2 Kg)	590 Hv	570 Hv	558 Hv
Imprint size (1–2 Kg)	25–80 $\mu\text{m}$	25–80 $\mu\text{m}$	25–80 $\mu\text{m}$
Cracking	fine, above 500 g	fine, above 2 kg	fine, above 500 g
Average crack length	50 $\mu\text{m}$	7 $\mu\text{m}$	25 $\mu\text{m}$
Toughness (2 Kg load) $K_{\text{Q}}$ (MPa $\sqrt{\text{m}}$ )	2.7 MPa $\sqrt{\text{m}}$	86 MPa $\sqrt{\text{m}}$	14 MPa $\sqrt{\text{m}}$

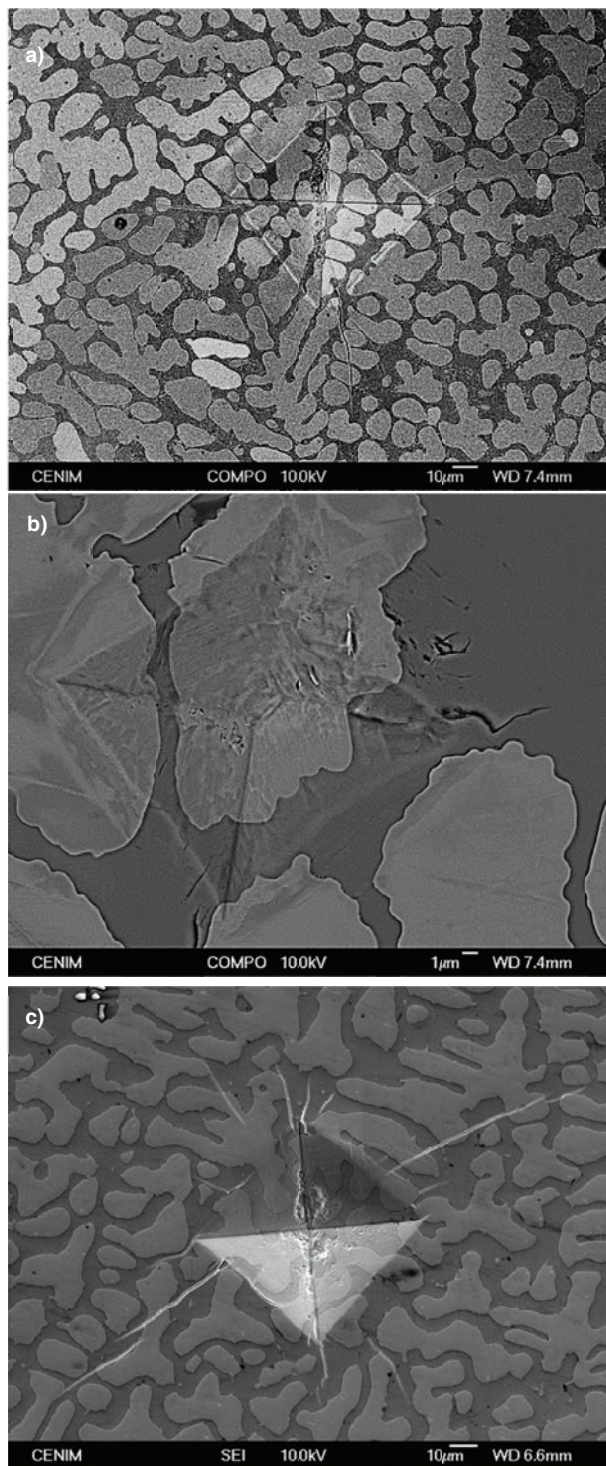


FIGURE 8. Examples of hardness imprints, all obtained with a load of 2 Kg, leading to crack formation: (a) back-scattered electron image showing alloy 1; (b) back-scattered electron image showing alloy 2; (c) secondary electron image showing alloy 3.

between various atoms, predicts the formation of single phase solid solutions or a mixture of solid solution with intermetallic phases for values lower

than 1.175 or higher, respectively. As seen in Table 4, this parameter is larger than the critical value for all three alloys, and hence correctly predicts that a mixture of solid solution with intermetallic should be obtained, as has been experimentally proved.

The thermodynamic predictions using *Thermocalc* software for the three alloys are shown in the Fig. 9. The vertical red lines corresponds to the composition of the three alloys in wt% (see Table 1)

In the case of HEA1 alloy, the solidus temperature is around 1550 °C and corresponds to the melting of the BCC1 phase. Below the liquidus and until about 880 °C a single BCC1 phase is stable, validating the prediction obtained with the more conventional criteria and confirming the hypothesis that this composition is appropriate for the formation of a single phase High Entropy Alloy. Below that temperature various secondary phases are formed. The first phase that appears to be thermodynamically stable is the AlSc intermetallic phase which is stable down to room temperature. For the HEA1 composition, at temperature below 800 °C the matrix BCC phase segregates and two BCC phases with different compositions are stable: BCC1 higher V and Cr contents and BCC2 that contains higher Ti and Al content. With decreasing temperature the BCC2 phase disappears and hexagonal Ti<sub>2</sub>Al and TiAl and are more thermodynamically stable.

However, there are some differences between the experimentally observed microstructure with the calculated. In the calculated phase diagram AlSc intermetallic phase appears to form, but Al<sub>2</sub>Sc intermetallic phase seems to be the only Al-Sc phase present in the alloy. Since the calculated BCC1 does not contain large amounts of Ti, intermetallic Ti-Al phases should be formed although it was not found in the interdendritic phase because Al is forming the Al<sub>2</sub>Sc intermetallic phase instead.

The liquidus temperature for HEA2 is 1668 °C. Below this temperature, the BCC1 single phase is stable down to 950 °C. This single BCC phase is a high entropy alloy. Below 950 °C the matrix cubic phases segregates into two cubic phases BCC1 and BCC2 and in addition and AlSc<sub>2</sub> intermetallic also appears to be stable. The BCC1 phase consists of Ti-Al Sc in similar amounts, whereas the BCC2 phase consists mainly of Cr and V. As temperature decrease AlSc intermetallic appears. In addition, BCC1 phase disappears and BCC3 phase appears. At lower temperature Ti and Al form the intermetallic phase Ti<sub>3</sub>Al and the BCC3 phase is no longer stable.

The phases experimentally observed for this alloy are a dendritic V-rich BCC phase and the intermetallic Al<sub>2</sub>Sc compound. Thermodynamic calculations predict the existence at low temperature of a V-Cr-rich phase, BCC2, as well as the AlSc intermetallic compound. This disagrees with experimental

TABLE 4. Mixing enthalpy ( $\Delta H$ ), atomic misfit ( $\delta$ ), mixing entropy ( $\Delta S$ ), valence electron concentration (VEC),  $\Omega$  and  $\gamma$  parameters calculated for the three alloys

Alloy/Parameter	$\Delta H$ (kJmol <sup>-1</sup> )	$\delta$ (%)	$\Delta S$ (JK <sup>-1</sup> mol <sup>-1</sup> )	VEC	$\Omega$	$\gamma$
Alloy 1	-20.32	6.37	12.51	4	1.04	1.30
Alloy 2	-12.2	7.67	12.51	4.6	1.9	1.31
Alloy 3	-18.26	6.58	11.85	4.1	1.09	1.30

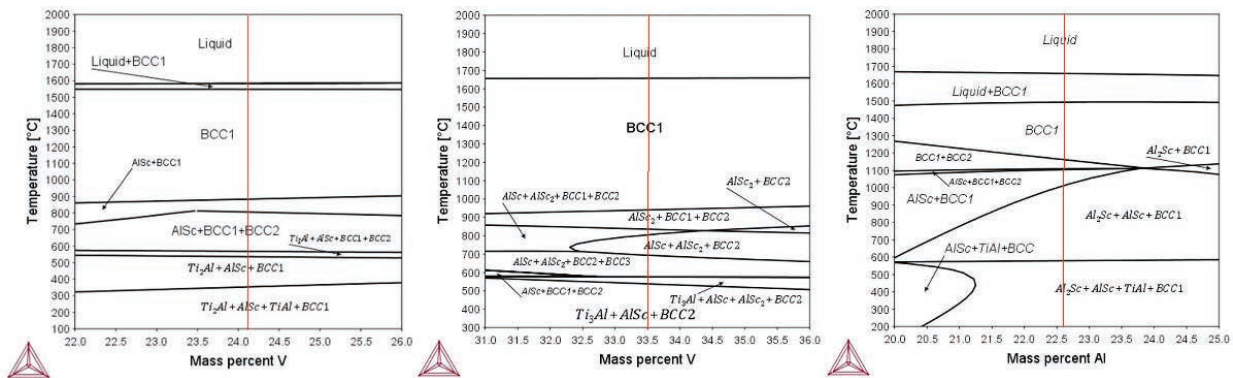


FIGURE 9. Quasi-binary phase diagrams Ti-V for Alloy 1, Cr-V for Alloy 2 and Al-V for Alloy 3.

observations, where  $Al_2Sc$  was detected in the interdendritic regions instead of  $AlSc$ . In addition, the presence of  $Ti_3Al$  intermetallic is also predicted, which is not observed experimentally. It appears that all the Ti is contained in the dendritic phase.

The solidus line for HEA3 occurs at 1500 °C and corresponds to melting of the single phase BCC1 phase. This single BCC1 phase is stable down to temperature of 1164 °C, where it segregates into two phases, BCC1 which is enriched in V and Al and BCC2 which contains mainly Sc, Al and Ti. At temperatures below 1100 °C the BCC2 phase disappears and the intermetallic  $AlSc$  appears, remaining stable down to room temperature. Also with decreasing temperature  $Al_2Sc$  and  $TiAl$  intermetallics appear to be thermodynamically stable. At low temperatures the phases that are stable are: V-rich BCC1 phase,  $AlSc$ ,  $Al_2Sc$  and  $TiAl$ .

The phases that are experimentally observed for this alloy are a dendritic Al-V phase and  $Al_2Sc$  intermetallic. Thermodynamic calculations predict correctly the formation of the  $Al_2Sc$  intermetallic. However, the thermodynamically stable BCC phase contains mainly V and therefore Ti forms the intermetallic  $TiAl$  phase, which is not observed experimentally. In addition, formation of  $AlSc$  is also predicted, which is not formed.

Similarly to previous HEA, DTA show an endothermic reaction at 1328 °C which does not

correspond to any transitions in the calculated phase diagram.

Considering the transitions observed in DTA for the three alloys, at temperatures that does not correspond to any transitions in the calculated phase diagram, it is postulated that the endothermic reactions corresponds to the dissolution of the  $Al_2Sc$  intermetallic

A comparison of hardness and toughness levels with the phase compositions and their relative volume allows some interpretation of the mechanical behavior. From Table 3, hardness of the dendrites increases in the sense alloy 2 – alloy 3 – alloy 1, with compositions (at. %) that correspond to the phases BCC-(41V-36Cr-12Al-9Ti) – BCC (48V-12Cr-25Al-13Ti) -BCC (37Ti-24V-24Al-10Cr). Here it would seem that Cr can play a role in softening the BCC solid solution, while Ti plays a significant hardening role. Furthermore, solid solution of Sc in dendrites seems to have also an important effect in reinforcing BCC solid solution phases. BCC-TiV solid solution dendrites in Alloy 1 dissolve 3 at.% of Sc whereas in BCC-AlV of alloy 3 and alloy 2 decreases to 1.5 at.% and 1 at.%, respectively. The differences in the atomic sizes of this three elements to Al and V have to affect the lattice distortion in BCC-solid solution. Such distortion will be more or less severe depending on the element and thus varying its reinforcing effect.

Hardness of alloys is very similar although increases in the sense of alloy 3-alloy 2-alloy 1. Therefore the alloy hardness has to be related to de volume fraction of BCC dendrites since it varies in the same sense.

Finally, the toughness measurements show that alloy 2 exhibits the highest value of 86 MPa m<sup>1/2</sup> whereas alloy 1 is the most brittle. These results can be only explained as a function of hardening and softening element content, Ti and Cr, as in the microhardness results. Thus, alloy 1 has the highest Ti content of 31.5% and the lowest Cr of 10% (Table 1). On the contrary, alloy 2 exhibits the lowest Ti content of 10 % and 28 % Cr whereas alloy 3 is in between both alloys.

## 5. CONCLUSIONS

The main conclusions of this research work are:

- The three alloys exhibit a two-phase microstructure with a considerable fraction of interdendritic second phase material.
- The major, dendritic phase in all three alloys could be considered as a High Entropy Phase, since it is a solid solution as follows:  $\alpha$  bcc solid solution rich in Ti, V for alloy 1, rich in V, Cr for alloy 2, and rich in Al, V for alloy 3. Sc is strongly rejected from the dendrites into the interdendritic material where it forms Al<sub>2</sub>Sc.
- The hardest bcc solid solution dendritic phase is that containing large amounts of Ti (Alloy 1), with the softest being the dendrites containing large amounts of Cr (Alloy 2).
- $\gamma$  parameter, in the cut-off value  $\gamma = 1.17$  explains perfectly the solid solution plus intermetallic structure of the three alloys studied.
- The thermodynamic predictions by using ThermoCalc software with SSOL5 database agree with those from the criteria used in this work for the formation of a single phase High Entropy Alloy although it has been shown that predictions do not match the experimental results.

## ACKNOWLEDGEMENTS

The authors would like to thank to J.F. Fernandez and J. Bodega belonging to MIRE-Group, of Dpto. Física de Materiales UAM, for alloys preparation. We would also like to acknowledge the expert support of A. García and A. Tomás of the CENIM Microscopy Laboratory. We want especially to thank the Profs. G. Morris and M.A. Muñoz for introducing us into the field of HEA alloys. Thanks to the X-ray Diffraction Laboratory. It is appreciated the financing of the Ministerio de Economía y Competitividad, through the RYC-2014-15014.

## REFERENCES

- Andersson, J.-O., Helander, T., Höglund, L., Shi, P., Sundman, B. (2002). Thermo-CALC & DICTRA, Computational tools for materials science. *Calphad* 26 (2), 273–312. [https://doi.org/10.1016/S0364-5916\(02\)00037-8](https://doi.org/10.1016/S0364-5916(02)00037-8).
- Anstis, G.R., Chantikul, P., Lawn, B.R., Marshall, D.B. (1981). A Critical Evaluation of Indentation Techniques for Measuring Fracture Toughness: I, Direct Crack Measurements. *Am. Ceram. Soc.* 64 (9), 533–538. <https://doi.org/10.1111/j.1151-2916.1981.tb10320.x>.
- Cantor, B. (2011). *High-entropy alloys*. In: *Encyclopedia of materials: Science and Technology*. K.H.J. Buschow, R.W. Cahn, M.C. Flemings, B. Ilshner, E.J. Kramer, S. Mahajan, P. Veyssiere (Editors), Elsevier, Pergamon, pp. 1.3. <https://doi.org/10.1016/B978-0-08-043152-9.02274-0>.
- Cantor, B., Chang, I.T.H., Knight, P., Vincent, A.J.B. (2004). Microstructural development in equiatomic multicomponent alloys. *Mat. Sci. Eng. A* 375–377, 213–218. <https://doi.org/10.1016/j.msea.2003.10.257>.
- Cantor, B., Audebert, F., Galano, M., Kim, K.B., Stone, I.C., Warren, P.J. (2005). Novel Multicomponent Alloys. *J. Metastab. Nanocryst. Mater.* 24–25, 1–6. <https://doi.org/10.4028/www.scientific.net/JMNM.24-25>.
- Fu, Z., Chen, W., Wen, H., Zhang, D., Chen, Z., Zheng, B., Zhou, Y., Lavernia, E.J. (2016). Microstructure and strengthening mechanisms in an FCC structured single-phase nanocrystalline Co<sub>25</sub>Ni<sub>25</sub>Fe<sub>25</sub>Al<sub>7.5</sub>Cu<sub>17.5</sub> high-entropy alloy. *Acta Mater.* 107, 59–71. <https://doi.org/10.1016/j.actamat.2016.01.050>.
- Guo, S., Liu, C.T. (2011). Phase stability in high entropy alloys: Formation of solid-solution phase or amorphous phase. *Prog. Nat. Sci.* 21 (6), 433–446. [https://doi.org/10.1016/S1002-0071\(12\)60080-X](https://doi.org/10.1016/S1002-0071(12)60080-X).
- Kumar, A., Gupta, M. (2016). An Insight into Evolution of Light Weight High Entropy Alloys: A Review. *Metals* 6 (9), 1–19. <https://doi.org/10.3390/met6090199>.
- Lu, Z.P., Wang, H., Chen, M.W., Baker, I., Yeh, J.W., Liu, C.T., Nieh, T.G. (2015). An assessment on the future development of high-entropy alloys: Summary from a recent workshop. *Intermetallics* 66, 67–76. <https://doi.org/10.1016/j.intermet.2015.06.021>.
- Miracle, D.B., Senkov, O.N. (2017). A critical review of high entropy alloys and related concepts. *Acta Mater.* 122, 448–511. <https://doi.org/10.1016/j.actamat.2016.08.081>.
- Morris, D.G., Leboeuf, M., Morris, M.A. (1998). Hardness and toughness of MoSi<sub>2</sub> and MoSi<sub>2</sub>-SiC composite prepared by reactive sintering of powders. *Mat. Sci. Eng. A* 251 (1–2), 262–268. [https://doi.org/10.1016/S0921-5093\(98\)00517-6](https://doi.org/10.1016/S0921-5093(98)00517-6).
- Pickering, E.J., Jones, N.G. (2016). High entropy alloys: a critical assessment of their founding principles and future prospects. *Int. Mater. Rev.* 61 (3), 183–202. <https://doi.org/10.1080/09506608.2016.1180020>.
- Poletti, M.G., Battezzati, L. (2014). Electronic and thermodynamic criteria for the occurrence of high entropy alloys in metallic systems. *Acta Mater.* 75, 297–306. <https://doi.org/10.1016/j.actamat.2014.04.033>.
- Ren, B., Liu, Z.X., Li, D.M., Shi, L., Cai, B., Wang, M.X. (2010). Effect of elemental interaction on microstructure of CuCrFeNiMn high entropy alloy system. *J. Alloy Compd.* 493 (1–2), 148–153. <https://doi.org/10.1016/j.jallcom.2009.12.183>.
- Takeuchi, A., Inoue, A. (2005). Classification of Bulk Metallic Glasses by Atomic Size Difference, Heat of Mixing and Period of Constituent Elements and Its Application to Characterization of the Main Alloying Element. *Mater. Trans.* 46 (12), 2817–2829. <https://doi.org/10.2320/matertrans.46.2817>.
- Toda-Caraballo, I., Rivera Díaz-del-Castillo, P.E. (2016). A criterion for the formation of high entropy alloys based on lattice distortion. *Intermetallics* 71, 76–87. <https://doi.org/10.1016/j.intermet.2015.12.011>.
- Wu, W.-H., Yang, C.C., Yeh, J.W. (2006). Industrial development of high-entropy alloys. *Ann. Chim. – Sci. Mat.* 31 (6), 737–747. <https://doi.org/10.3166/acsm.31.737-747>.

- Yang, X., Zhang, Y. (2012) Prediction of high-entropy stabilized solid-solution in multi-component alloys. *Mater. Chem. Phys.* 132 (2–3), 233–238. <https://doi.org/10.1016/j.matchemphys.2011.11.021>.
- Yang, X., Zhang, Y., Liaw, P.K. (2012). Microstructure and Compressive Properties of NbTiVTaAlx High Entropy Alloys. *Procedia Engineer.* 36, 292–298. <https://doi.org/10.1016/j.proeng.2012.03.043>.
- Ye, Y.F., Liu, C.T., Yang, Y. (2015). A geometric model for intrinsic residual strain and phase stability in high entropy alloys. *Acta Mater.* 94, 152–161. <https://doi.org/10.1016/j.actamat.2015.04.051>.
- Yeh, J.W., Chen, S.K., Lin, S.J., Gan, J.Y., Chin, T.S., Shun, T.T., Tsau, C.H., Chang, S.Y. (2004). Nanostructured High-Entropy Alloys with Multiple Principal Elements: Novel Alloy Design Concepts and Outcomes. *Adv. Eng. Mater.* 6 (5), 299–303. <https://doi.org/10.1002/adem.200300567>.
- Youssef, K.M., Zaddach, A.J., Niu, C., Irving, D.L., Koch, C.C. (2015). A Novel Low-Density, High-Hardness, High-entropy Alloy with Close-packed Single-phase Nanocrystalline Structures. *Mater. Res. Lett.* 3 (2), 95–99. <https://doi.org/10.1080/21663831.2014.985855>.
- Yue, M.T., Xie, H., Lin, X., Yang, H., Meng, G. (2013). Microstructure of Laser Re-Melted AlCoCrCuFeNi High Entropy Alloy Coatings Produced by Plasma Spraying. *Entropy* 15 (7), 2833–2845. <https://doi.org/10.3390/e15072833>.
- Zhang, Y., Zhou, Y.J., Lin, J.P., Chen, G.L., Liaw, P.K. (2008). Solid-Solution Phase Formation Rules for Multi-component Alloys. *Adv. Eng. Mater.* 10 (6), 534–538. <https://doi.org/10.1002/adem.200700240>.
- Zhang, K., Fu, Z. (2012). Effects of annealing treatment on phase composition and microstructure of CoCrFeNiTiAlx high-entropy alloys. *Intermetallics* 22, 24–32. <https://doi.org/10.1016/j.intermet.2011.10.010>.
- Zhang, Y., Yang, X., Liaw, P.K. (2012). Alloy Design and Properties Optimization of High-Entropy Alloys. *JOM* 64 (7), 830–838. <https://doi.org/10.1007/s11837-012-0366-5>.
- Zhang, Y., Zuo, T.T., Tang, Z., Gao, M.C., Dahmen, K.A., Liaw, P.K., Lu, Z.P. (2014). Microstructures and properties of high-entropy alloys. *Prog. Mater. Sci.* 61, 1–93. <https://doi.org/10.1016/j.pmatsci.2013.10.001>.